Supporting Material: Cholesterol modulates CFTR confinement in the plasma membrane of primary epithelial cells

Asmahan Abu-Arish
Physics and Physiology,
McGill University, Montreal, QC

Elvis Pandzic
Physics,
McGill University, Montreal, QC

Julie Goepp
Physiology,
McGill University, Montreal, QC

Elizabeth Matthes
Physiology,
McGill University, Montreal, QC

John W. Hanrahan
Physiology,
McGill University, Montreal, QC

Paul W. Wiseman [1]
Chemistry & Physics,
McGill University, Montreal, QC

[1]Corresponding author. Address: Physics, McGill University, 3600 Rue University, Montreal, QC H3A2T8, Canada., Tel.: (514)398-5354, Fax: (514)398-8434

Supporting Materials and Methods

Isolation and culture of human bronchial epithelial (HBE) primary cells:

Human lung tissues were obtained from non-CF and CF individuals after lung transplantation with informed consent under a protocol approved by the Institutional Review Board of the Research Ethics Office of McGill University. Isolation and culture of HBE cells were adapted from procedures previously described (1, 2). Briefly, non-CF and CF airway epithelial cells were isolated from bronchial tissue by enzymatic digestion and were cultured in bronchial epithelial growth medium (BEGM; (1)) on Vitrogen-coated plastic flasks (Advanced BioMatrix, San Diego, CA), then trypsinized, counted, and cryopreserved or transferred directly onto Vitrogen-coated glass-bottom FluoroDishes (4.34 cm^2, World Precision Instruments, Inc. Sarasota, FL) adapted for imaging at a density of 3×10^5 cells/dish. Fresh or previously cryopreserved passage 1 (P1) cells were used. The BEGM medium was changed every two days for a total of 4 days. At 80% confluency, cells were ready to be infected with GFP-CFTR containing adeno-virus as detailed in the paper. For the CF HBE cells, the isolation and growth media were supplemented with specific and adapted antibiotics based on a recent patient antibiogram.

Preparation of membrane patches:

The preparation of membrane patches was done according to (3). Briefly, HBE cells expressing GFP-CFTR grown on 35 mm collagen-coated glass-bottom FluoroDishes were sheared by sonication in ice-cold PBS-buffer using a 100 ms ultrasound pulse. This resulted in removal of cell content except for the basal plasma membrane, which remained attached to the glass-bottom of the FluoroDish and is referred to as a membrane patch. After the procedure, membrane patches were rinsed three times and kept at 4°C in PBS until imaging. The patches were imaged at room temperature using an LSM-710 (Zeiss, Germany).

Transferrin internalization assay:

For live cell imaging of fluorescent-transferrin to reveal clathrin-coated pits (CCPs), HBE cells were serum-starved in OptiMEM for 18 hours at 37°C, then treated acutely with 50 μg/mL of Alexa-594 labeled transferrin (Molecular Probes) for

30 min at 37°C. The cells were then rinsed, mounted in transferrin-free Opti-MEM medium and transferred to the microscope where they were kept at 37°C to monitor transferrin receptor accumulation in CCPs. Samples were imaged using the 488 nm and 561 nm laser lines simultaneously for fluorescence colocalization studies.

Cell fixation:

HBE cells were rinsed twice in 37°C PBS, then incubated with neutral buffered formalin (10%) (Harleco) for 1 hour at room temperature and maintained at 4°C overnight. The next morning, the cells were rinsed twice for 5 min with cold PBS and stored in PBS at 4°C until imaged. Cells were imaged at 37°C to maintain similar imaging conditions for comparison with live cells results.

Spatial image cross-correlation spectroscopy (ICCS):

Two-color ICCS was used to assess the colocalized fractions of GFP-CFTR clusters and fluorescent-transferrin-labeled CCPs (4, 5). Colocalization fractions for a region of interest (ROI) were calculated as the ratio of the amplitudes of the spatial cross-correlation and autocorrelation functions determined from CLSM images from the green (g) and red (r) detection channels. The number of colocalized particles (clusters) per beam area was determined as follows:

$$<N>_{gr} = \frac{r(0,0)_{gr}}{r(0,0)_{gg} r(0,0)_{rr}} \frac{A_r}{A_g} \tag{1}$$

where r(0,0) is the zero lags best-fit amplitude of the spatial autocorrelation (gg and rr) or cross-correlation (gr) functions, and $A_{r/g}$ is the effective area of the focal spot for each laser. The ICCS interaction fraction was defined as the ratio of the number of interacting particles to the total number of fluorescently labeled particles in each detection channel:

$$M_{CFTR} = \frac{r(0,0)_{gr}}{r(0,0)_{gg}} = \frac{<N>_{gr}}{<N>_{rr}} \tag{2}$$

and,

$$M_{CCP} = \frac{r(0,0)_{gr}}{r(0,0)_{rr}} = \frac{<N>_{gr}}{<N>_{gg}} \tag{3}$$

where GFP-CFTR was collected in the g channel and CCPs (Alexa-594 transferrin) in the r channel. Analysis was performed on a large ROI inside the cells. Spatial ICCS provides information about the colocalization of clusters rather than single molecules for an aggregated system. About 50 cells were analyzed.

Supporting Results

GFP-CFTR signal versus autofluorescence:

Fluorescence confocal microscopy images of HBE cells transiently expressing GFP-CFTR on the plasma membrane showed the presence of two different CFTR populations: a population in clusters and a diffuse population in areas outside of clusters. Confocal images of HBE cells expressing GFP-CFTR were compared to images of non-expressing cells (autofluorescence control). Fig. S1 shows a large field of view containing an HBE cell expressing GFP-CFTR (red arrow) next to several other cells that do not express the protein (yellow arrows). It is clear that autofluorescence in cells devoid of GFP-CFTR is negligible compared to the fluorescence generated by the expression of GFP-CFTR.

Fixed cells analysis:

As a negative control for the kICS analysis, untreated and fixed HBE cells expressing GFP-CFTR were imaged and analyzed in a similar manner to untreated live cells. Protein diffusion is arrested in fixed cells, thus fixation establishes the minimum detection limits for kICS transport measurements and the R value due to mechanical noise arising from random thermal drift of the microscope stage and sample.

Fig. S2 shows the circularly averaged correlation function for GFP-CFTR in live and fixed cells as a function of k^2 at different temporal lags. The correlation functions of GFP-CFTR under live and fixed cell conditions show clear differences in decay rates as expected. The average correlation function of CFTR from the live cells decays as a function of time (from blue to red) indicating protein mobility whereas the correlation function from fixed cells shows no clear decay in time indicative of immobile CFTR. Fig. S3 shows the average micro MSD versus τ graph for fixed and live measurements. The slope of the first 3 temporal lags of the micro MSD for the fixed cells is dramatically smaller than the live cells which indicates a significantly smaller D_{micro} for the fixed cells as expected

due to fixation (table S1). Moreover, a significant difference in the intercept of the $D_{micro}\tau$ axis at large time lags indicates a much smaller R value for fixed cell measurements (table S1). The smaller R value is indicative of a higher degree of confinement as expected from fixed molecules which are cross-linked.

Parameter interdependency:

Fig. S4a shows a schematic drawing of a 2D trajectory of an individual CFTR channel undergoing transiently confined dynamics on the plasma membrane of live cells. The black trajectory represents CFTR transport dynamics in the membrane outside of confinements (microdomains, yellow discs), while the red trajectory is the movement of confined CFTR inside the microdomains, which is referred to in this study as micro dynamics. The kICS analysis yields D_{micro}: the recovered diffusion coefficient inside the confinements. Fig. S4b shows the macroscale trajectory of CFTR in the plasma membrane (blue) which is referred to as the macro scale dynamics of CFTR. The recovered diffusion coefficient by kICS is D_{macro}.

D_{macro} is affected by several factors as established by simulations (6). To summarize, a decrease in the recovered D_{macro} can be due to an increase in the viscosity of the membrane, an increase in the density of microdomains, or a decrease in the escape probability of particles from confinements. For systems with populations in kinetic exchange between confinements, D_{macro} is an effective (not absolute) macro scale diffusion coefficient as it is partially coupled to D_{micro} depending on the dynamic parameters of confinement and exchange. Simulations (6) show that D_{micro} is affected by several factors as well, but is independent of D_{macro}. To summarize, a decrease in D_{micro} reflects an increase in the viscosity of domains, a decrease in the escape probability of particles from domains, or an increase in domain radii. Overall, an increase in CFTR confinement is expected to decrease both D_{macro} and D_{micro}.

CFTR clusters are on the plasma membrane according to the membrane-patch method:

To determine if CFTR clusters were localized to the plasma membrane or attached to a structure within the cell (such as the actin-cytoskeleton), membrane patches were prepared from HBE cells expressing GFP-CFTR as described in Materials and Methods and immediately imaged (Fig. S5). The imaged CFTR distribu-

tion was similar to that on the basal membrane of live cells for all membrane patches imaged indicating that CFTR clusters are attached to the plasma membrane. To rule out the possibility that these clusters are associated with residual components of the actin-cytoskeleton, samples were fluorescently labeled with phalloidon-Alexa555 to label F-actin. Images of phalloidin labeled membrane patches did not reveal any F-actin on the patches (data not shown). Our results suggest that CFTR clusters are aggregates of CFTR molecules within the plasma membrane, consistent with their ion channel function.

CFTR clusters are not clathrin-coated pits:

It has been previously shown that CFTR is internalized through clathrin-coated pits (CCPs) (7). To test whether CFTR clusters are CCP internalization sites of CFTR, a fluorescent-transferrin internalization assay was performed to fluorescently label CCPs (8, 9), followed by a fluorescent colocalization study between GFP-CFTR clusters and labeled CCPs using Image Cross Correlation Spectroscopy (ICCS) analysis. Live HBE cells expressing GFP-CFTR were treated with a fluorescently labeled transferrin receptor (TfR) ligand (transferrin-Alex594) as detailed in Materials and Methods. Upon binding its receptor, transferrin stimulates the internalization of TfR through CCPs and results in fluorescent labeling of the coated pits. Fluorescently labeled CCPs were homogeneously distributed as shown in Fig. S6 (white arrows). Approximately 20% of the CFTR clusters were colocalized with CCPs according to ICCS analysis suggesting that only a small percentage of CFTR clusters are situated at these sites of endocytosis.

Supporting References

1. Fulcher, M. L., S. Gabriel, K. A. Burns, J. R. Yankaskas, and S. H. Randell, 2005. Well-Differentiated Human Airway Epithelial Cell Culture. *Methods Mol Med* 107:183–206.

2. Randell, S. H., L. Walstad, U. E. Schwab, B. R. Grubb, and J. R. Yankaskas, 2001. Isolation and Culture of Airway Epithelial Cells from Chronically Infected Human Lungs. *In Vitro Cell Dev Biol Anim* 37:480–489.

3. Avery, J., D. J. Ellis, T. Lang, P. Holroyd, D. Riedel, R. M. Henderson, J. M. Edwardson, and R. Jahn, 2000. A cell-free system for regulated exocytosis in PC12 cells. *J. Cell Biol.* 148:317–324.

4. Comeau, J. W. D., S. Costantino, and P. W. Wiseman, 2006. A Guide to Accurate Fluorescence Microscopy Colocalization Measurements. *Biophys J* 91:4611–4622.

5. Wiseman, P. W., J. A. Squier, M. H. Ellisman, and K. R. Wilson, 2000. Two-Photon Image Correlation Spectroscopy and Image Cross-Correlation Spectroscopy. *J Microsc* 200:14–25.

6. Pandzic, E., 2013. Confinement in Image correlation Spectoscopy. Ph.D. thesis, McGill University, Montreal, Canada.

7. Bradbury, N. A., J. A. Clark, S. C. Watkins, C. C. Widnell, H. S. S. IV, and R. J. Bridges, 1999. Characterization of the internalization pathways for the cystic fibrosis transmembrane conductance regulator. *Am. J. Physiol. Lung Cell Mol. Physiol.* 276:L659–L668.

8. Santini, F., and J. H. Keen, 1996. Endocytosis of Activated Receptors and Clathrin-coated Pit Formation: Deciphering the Chicken or Egg Relationship. *The Journal of Cell Biology* 132:1025–1036.

9. Prigozhina, N. L., and C. M. Waterman-Storer, 2006. Decreased polarity and increased random motility in PtK1 epithelial cells correlate with inhibition of endosomal recycling. *Journal of Cell Science* 119:3571–3582.

Supporting Tables

Table S 1: CFTR confinement parameters measured using kICS analysis

Treatment	$D_{micro}(\mu m^2/s)$	$D_{macro}(\mu m^2/s)$	R (μm)	n_{cell}
Live	0.009±0.001	0.014±0.003	0.293±0.005	136
Fixed	0.0005±0.0002†	0.0010±0.0003†	0.236±0.002†	151

(†) significantly different than live cells, p <0.001

Supporting Figures

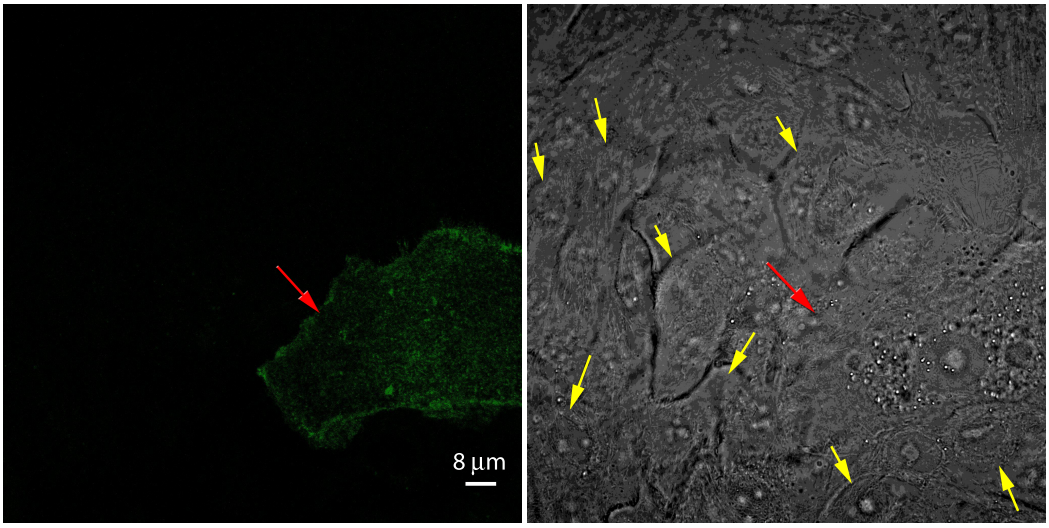

(a) Fluorescence confocal image (b) Transmitted Light image

Figure S 1: The fluorescence produced by GFP-CFTR expression is readily distinguished from autofluorescence. (a) Fluorescence confocal image of HBE cells transiently expressing GFP-CFTR (red *arrow*). (b) Transmitted light image of the same region of interest. Comparing cells with (red *arrow*) and without (yellow *arrow*) GFP-CFTR clearly shows that autofluorescence is negligible.

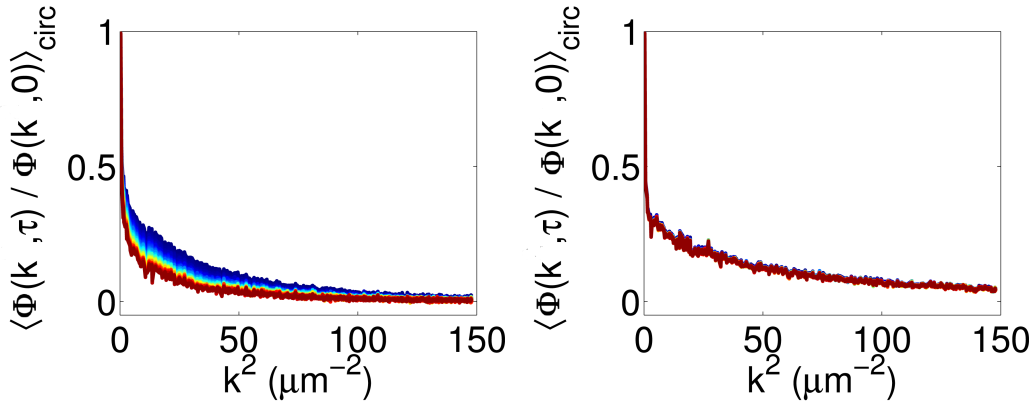

(a) Live cells (b) Fixed cells

Figure S 2: Control: normalized and circularly-averaged k-space correlation function for GFP-CFTR measured on fixed HBE cells establishes the transport parameter detection limit for this optical system. (a) The average correlation function for GFP-CFTR measured on live cells as a function of the spatial frequency (k^2), for different temporal lags. The average spatial correlation function decays as a function of τ (blue to red) due to CFTR mobility in the membrane. The presence of at least two dynamically distinct populations is evident in both the early (blue) and the late (red) temporal lag spatial correlations. (b) The average correlation function for GFP-CFTR from fixed cells as a function of k^2 for different time lags. No decay in the spatial correlation function in time is observed indicative of CFTR immobility due to cell fixation. See also Supporting Table 1.

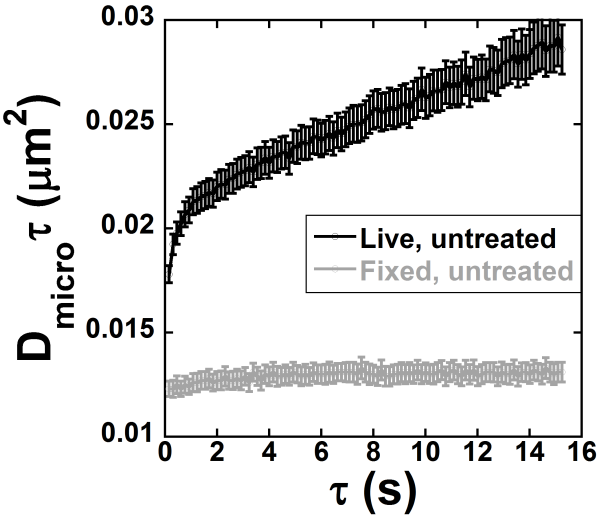

Figure S 3: CFTR micro dynamics on the plasma membrane of live and fixed HBE cells. The average micro scale MSD, $D_{micro}\tau$, of CFTR increased linearly as a function of τ for the first few temporal lags in live cells (black) due to CFTR mobility. No significant increase in the MSD for fixed cells was observed (gray) indicative of immobile CFTR as expected. Error bars are SEM.

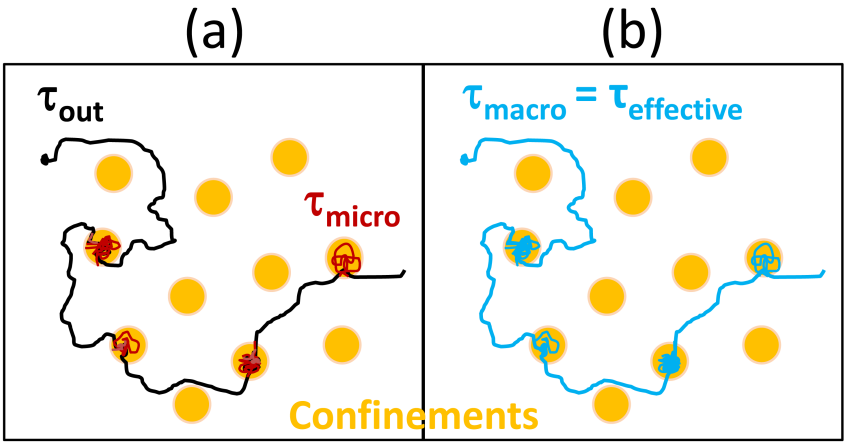

Figure S 4: A schematic drawing of the measured transport dynamics parameters probed via kICS. (a) A 2D trajectory of an individual CFTR channel on the plasma membrane of live cells. The black trajectory describes CFTR transport dynamics outside of confinements (yellow discs), while the red trajectory is the movement of confined CFTR inside the microdomains, that we term micro dynamics. The recovered diffusion coefficient inside the confinements is D_{micro}. (b) The macroscale trajectory of CFTR in the plasma membrane (blue) that we term macro, but it is also coupled via particle exchange to the micro scale dynamics. The recovered diffusion coefficient by kICS is D_{macro}.

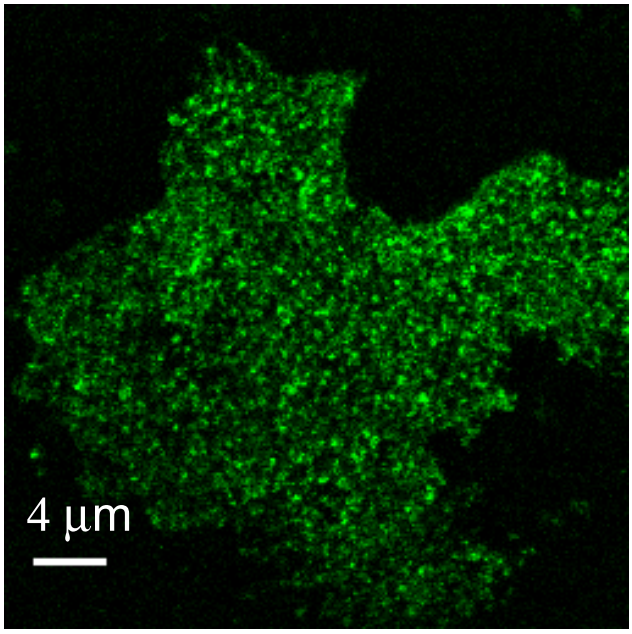

Figure S 5: GFP-CFTR distribution on a plasma membrane patch is similar to that on the basal membrane of live cells. The clear presence of CFTR clusters suggests their insertion in the plasma membrane.

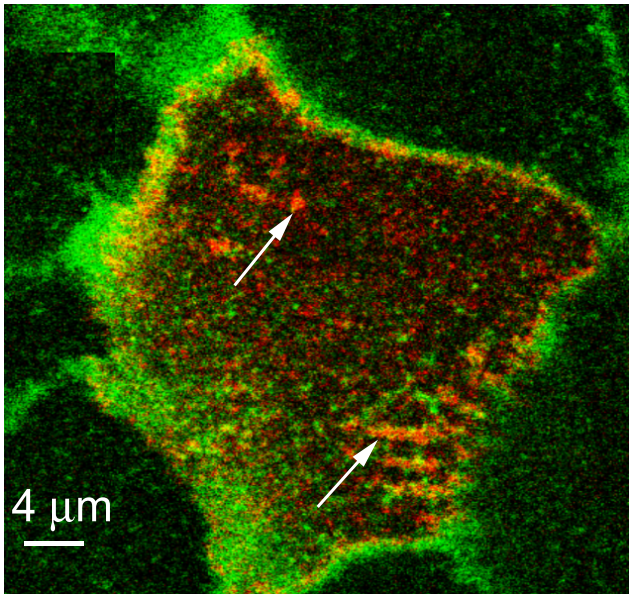

Figure S 6: The majority of CFTR clusters are not situated at CCPs and therefore are not undergoing clathrin mediated endocytosis. ICCS analysis revealed that only 20% of CFTR clusters (green) spatially colocalize with CCP internalization sites (red) while the majority of the clusters do not overlap with the labeled CCP sites. White arrows mark examples of colocalization sites.

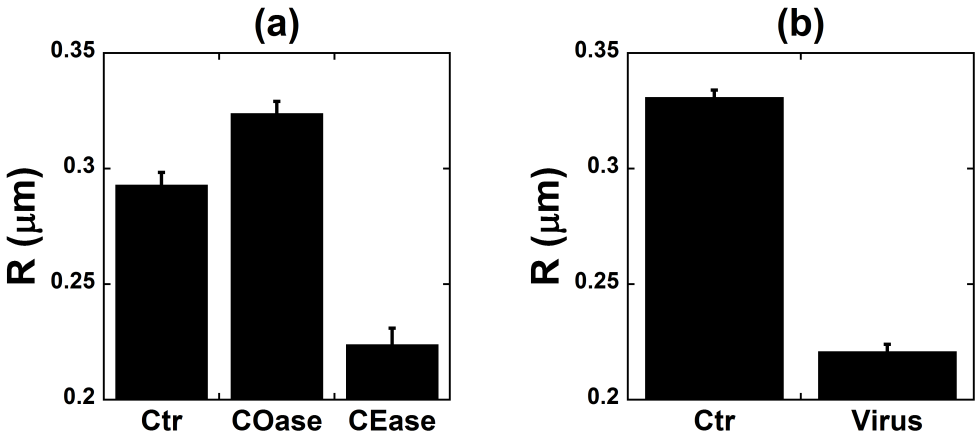

Figure S 7: CFTR confinement strength is cholesterol-dependent. (a) Cholesterol loss by COase treatment resulted in a significant increase in the average R value, consistent with an increase in the exchange dynamics of CFTR in and out of confinements. Cholesterol insertion by CEase treatment resulted in a dramatic decrease in the average R value, consistent with an increase in CFTR confinement and tethering. (b) CFTR confinement strength increased immediately after adenovirus infection. The decrease in the average R value after acute infection indicates an increase in CFTR tethering and confinement in the newly-formed platforms. Error bars are SEM.